Nonlinear standing waves in an acoustical resonator

Yurii A. Ilinskii, Bart Lipkens, Timothy S. Lucas, Thomas W. Van Doren, and Evgenia A. Zabolotskaya
MacroSonix Corporation, 1570 East Parham Road, Richmond, Virginia 23228

(Received 6 November 1997; revised 31 July 1998; accepted 3 August 1998)

A one-dimensional model is developed to analyze nonlinear standing waves in an acoustical resonator. The time domain model equation is derived from the fundamental gasdynamics equations for an ideal gas. Attenuation associated with viscosity is included. The resonator is assumed to be of an axisymmetric, but otherwise arbitrary shape. In the model the entire resonator is driven harmonically with an acceleration of constant amplitude. The nonlinear spectral equations are integrated numerically. Results are presented for three geometries: a cylinder, a cone, and a bulb. Theoretical predictions describe the amplitude related resonance frequency shift, hysteresis effects, and waveform distortion. Both resonance hardening and softening behavior are observed and reveal dependence on resonator geometry. Waveform distortion depends on the amplitude of oscillation and the resonator shape. A comparison of measured and calculated wave shapes shows good agreement. © *1998 Acoustical Society of America.* [S0001-4966(98)02711-8]

PACS numbers: 43.25.Gf [MAB]

INTRODUCTION

The resonant macrosonic synthesis technology developed at MacroSonix Corp. involves acoustic standing waves of very high amplitude with peak acoustic pressures that exceed the ambient pressure 3–4 times.[1] When the acoustic pressure is so high, the standing waves are strongly nonlinear, and phenomena such as resonance frequency shift, hysteresis effects, and harmonic generation take place and can be observed. Power is delivered to the resonator by a motor that shakes the entire cavity.

Most of the experimental and theoretical studies reported in the literature are limited to finite-amplitude standing waves in tubes of constant cross section with a piston excitation at one end and a rigid cap at the other. Saenger and Hudson,[2] Weiner,[3] and Temkin[4] assumed in their analysis that the wavefront consists of discontinuous shock fronts connected by a continuous section. Chester[5] introduced a second order theoretical analysis that included the effects of boundary layer and volume absorption. Cruikshank[6] compared measurements in a tube with Chester's predictions and found good qualitative agreement. Coppens and Sanders[7] presented a perturbation expansion for a one-dimensional second order nonlinear wave equation, which they extended later to a three-dimensional model for lossy cavities.[8] A single nonlinear equation was used to describe the finite-amplitude standing waves in a cavity. Linear resonance frequencies and quality factors are used to predict the amplitude of the higher harmonics of the finite-amplitude wave. Gaitan and Atchley[9] used the model of Coppens and Sanders to study finite-amplitude standing waves in so-called harmonic and anharmonic tubes. The harmonic tube was a cylinder, while the anharmonic tube consisted of a cylindrical tube with a midsection that had an expansion or a contraction. The measurements showed good agreement with the model. It was also found that the tubes with nonequidistant modal spectra effectively suppressed the energy transfer from the fundamental to the higher harmonics.

Gaitan and Atchley use the term ''harmonic tubes'' to describe resonators for which the harmonics of the fundamental resonance coincide with the higher resonance frequencies. The term ''anharmonic tube'' is used to describe a resonator for which the harmonics of the fundamental do not coincide with the higher resonance frequencies. This terminology is essentially based on linear parameters. However, confusion can arise, since the term ''anharmonic'' has been used in literature to describe a nonlinear oscillator (see, for example, the book by Goldstein).[10] Therefore we introduce the following terminology: (1) a resonator with an equidistant spectrum, i.e., higher resonances are integer multiples of the fundamental resonance, is called a consonant resonator; and (2) a resonator with a nonequidistant spectrum is called a dissonant resonator. The term ''consonance'' is also used by Coppens and Atchley[11] in their review article on nonlinear standing waves in cavities.

In this paper we introduce a one-dimensional mathematical model that has been developed at MacroSonix to analyze standing waves of high amplitude. The model is based on the nonlinear gas dynamics equations for an ideal gas inside a resonator that is axisymmetric, but otherwise has an arbitrary shape. An external harmonic force shakes the entire resonator cavity and excites the gas oscillation. Losses are introduced through bulk viscosity. The model provides insight into the physics of nonlinear standing waves in resonators of different shape and gives a tool to design resonators that have characteristics suitable for specific applications.

First, in order to study the strongly nonlinear 1D standing waves in the resonator, the time domain basic equation for the velocity potential is derived from the fundamental gasdynamic equations for potential motion of a perfect gas. The equation includes the total nonlinearity of gas and gas dynamic equations, the effects of volume absorption, the external force that shakes the entire resonator, and the resonator radius that varies along the resonator axis. Then the basic equation is prepared for numerical calculations: dimension-

less variables are introduced, the single equation is replaced by the set of two lower order equations, and the set of equations in the time domain is transformed into the spectral equations. N harmonics and the dc component are considered. The equations for the complex amplitudes of spectral components are integrated numerically. In the numerical calculations up to 20 harmonics are taken into account. Several acoustic variables are calculated. First, the harmonic amplitudes of the velocity potential wave are obtained directly from the solution of the frequency domain equations. Second, the shape of the pressure wave is calculated for different coordinates along the resonator axis. Last, a Fourier transform is performed to find the harmonic amplitudes of the pressure wave and the harmonic amplitude distributions along the resonator axis. Three resonator geometries are chosen to demonstrate the results: a cylinder, a cone, and a bulb.

I. BASIC EQUATIONS

Let us consider the one-dimensional acoustic wave field in a resonator of arbitrary axisymmetric shape. The entire resonator is oscillated along its axis by an external force supplied by a motor.

Three equations are required to describe the motion of a viscous gas in the acoustical resonator: (1) the mass conservation equation, (2) the momentum conservation equation, and (3) the state equation.

The mass conservation equation for the resonator with the radius that is variable with the coordinate along the resonator axis may be written in the form

$$\frac{\partial M}{\partial t}+\frac{\partial F}{\partial x}=0. \tag{1}$$

Here the following notations are introduced: M is a mass per unit length, F is a mass flux through the resonator cross section of the radius r, t is time, and x is a coordinate along the resonator. The radius is a function of x

$$r=r(x). \tag{2}$$

The resonator oscillates in the x direction.

In this case, the mass of gas per length unit and its flow through the cross section of radius r are equal to

$$M=\rho\pi r^2, \tag{3}$$

$$F=\rho u\pi r^2, \tag{4}$$

where ρ is the mass density and u is a particle velocity in the x direction.

After substituting Eqs. (3) and (4) into Eq. (1) we obtain the continuity equation for the gas in the resonator of the axisymmetric, but otherwise arbitrary shape:

$$\frac{\partial\rho}{\partial t}+\frac{1}{r^2}\frac{\partial}{\partial x}(r^2\rho u)=0. \tag{5}$$

The momentum equation for one-dimensional motion is

$$\frac{\partial u}{\partial t}+u\frac{\partial u}{\partial x}=-\frac{1}{\rho}\frac{\partial p}{\partial x}-a(t)+\frac{(\zeta+4\eta/3)}{\rho}\frac{\partial}{\partial x}\left(\frac{1}{r^2}\frac{\partial}{\partial x}(r^2u)\right). \tag{6}$$

Here, p is the pressure, $a(t)$ is the acceleration of the resonator, and ζ and η are coefficients of viscosity. All of these equations are written in the coordinate system that is moving with the resonator body.

A few words should be said about the dissipative term [the last term on the right-hand side of Eq. (6)]. In general, the dissipative term in the equation for the i velocity component can be presented in the three-dimensional form (see, for example, Landau and Lifshitz[12])

$$\eta\frac{\partial^2 u_i}{\partial x_k\,\partial x_k}+\left(\zeta+\frac{1}{3}\eta\right)\frac{\partial^2 u_k}{\partial x_i\,\partial x_k}. \tag{7}$$

For the velocity potential φ introduced as

$$u_i=\frac{\partial\varphi}{\partial x_i}, \tag{8}$$

Eq. (7) takes the form

$$\eta\frac{\partial^3\varphi}{\partial x_i\,\partial x_k\,\partial x_k}+\left(\zeta+\frac{1}{3}\eta\right)\frac{\partial^3\varphi}{\partial x_i\,\partial x_k\,\partial x_k}=\left(\zeta+\frac{4}{3}\eta\right)\frac{\partial^3\varphi}{\partial x_i\,\partial x_k\,\partial x_k}. \tag{9}$$

After integrating Eq. (9) over x_i and equating the arbitrary function to 0 we obtain

$$\left(\zeta+\frac{4}{3}\eta\right)\frac{\partial^2\varphi}{\partial x_k\,\partial x_k}=\left(\zeta+\frac{4}{3}\eta\right)\frac{\partial u_k}{\partial x_k}=\left(\zeta+\frac{4}{3}\eta\right)\nabla\cdot u. \tag{10}$$

The term $\nabla\cdot u$ should be written in the one-dimensional form of Eq. (5)

$$\nabla\cdot u=\frac{1}{r^2}\frac{\partial}{\partial x}(r^2u). \tag{11}$$

Combination of Eqs. (10) and (11) yields the dissipative term as written in Eq. (6).

The state equation is taken for an ideal gas

$$p=p_0\left(\frac{\rho}{\rho_0}\right)^{\gamma}, \tag{12}$$

where p_0, ρ_0 are ambient values of the pressure and density and γ is the ratio of specific heats.

Equation (6) written through the velocity potential φ takes the form

$$\frac{\partial^2\varphi}{\partial t\,\partial x}+\frac{1}{2}\frac{\partial}{\partial x}\left(\frac{\partial\varphi}{\partial x}\right)^2=-\frac{1}{\rho}\frac{\partial p}{\partial x}-a(t)+\frac{(\zeta+4\eta/3)}{\rho}\frac{\partial}{\partial x}\left(\frac{1}{r^2}\frac{\partial}{\partial x}\left(r^2\frac{\partial\varphi}{\partial x}\right)\right). \tag{13}$$

After substituting p from Eq. (12) into Eq. (13) and integrating over x we obtain

$$\frac{\partial\varphi}{\partial t}+\frac{1}{2}\left(\frac{\partial\varphi}{\partial x}\right)^2=-\frac{\gamma p_0}{(\gamma-1)\rho_0^{\gamma}}\,\rho^{(\gamma-1)}-a(t)x+\frac{\delta}{r^2}\frac{\partial}{\partial x}\left(r^2\frac{\partial\varphi}{\partial x}\right)+\phi(t). \tag{14}$$

Here, $\phi(t)$ is an arbitrary function of time and δ is

$$\delta=\frac{(\zeta+4\,\eta/3)}{\rho_0}. \tag{15}$$

The replacement of ρ by ρ_0 in the dissipative term means that the nonlinear terms that include absorption are ignored. This assumption states that the energy dissipation is small.

It is worth noting that the propagation speed c is equal to

$$c^2=\frac{dp}{d\rho}=\frac{\gamma p_0}{\rho_0^{\gamma}}\,\rho^{(\gamma-1)}. \tag{16}$$

The arbitrary function $\phi(t)$ in Eq. (14) is chosen as

$$\phi(t)=\text{const}. \tag{17}$$

Since the velocity potential φ is determined with the precision up to an arbitrary function of time, and we are interested in solutions that are periodic in time, we can add any periodic function to the potential to choose the proper solution; the only thing that cannot be compensated in this way is the dc component of the function ϕ. That's why we put ϕ as written by Eq. (17) where const is chosen to have the linear case in the limit when ρ approaches ρ_0,

$$\text{const}=\frac{c_0^2}{\gamma-1}. \tag{18}$$

Here c_0 is the small signal propagation speed. Equation (14) then takes the form

$$\frac{\partial\varphi}{\partial t}+\frac{1}{2}\left(\frac{\partial\varphi}{\partial x}\right)^2=-\frac{c^2-c_0^2}{\gamma-1}-a(t)x+\frac{\delta}{r^2}\frac{\partial}{\partial x}\left(r^2\frac{\partial\varphi}{\partial x}\right). \tag{19}$$

Differentiation of Eq. (14) with respect to t gives

$$\frac{\partial^2\varphi}{\partial t^2}+\frac{1}{2}\frac{\partial}{\partial t}\left(\frac{\partial\varphi}{\partial x}\right)^2=-\frac{\gamma p_0}{\rho_0^{\gamma}}\,\rho^{(\gamma-2)}\frac{\partial\rho}{\partial t}-\frac{da}{dt}\,x+\frac{\delta}{r^2}\frac{\partial^2}{\partial t\,\partial x}\left(r^2\frac{\partial\varphi}{\partial x}\right). \tag{20}$$

The derivative $\partial\rho/\partial t$ can be eliminated from Eq. (20) by using Eq. (5) in the form

$$\frac{\partial\rho}{\partial t}=-\frac{1}{r^2}\frac{\partial}{\partial x}\left(r^2\rho\,\frac{\partial\varphi}{\partial x}\right)=-\frac{\partial\rho}{\partial x}\frac{\partial\varphi}{\partial x}-\frac{\rho}{r^2}\frac{\partial}{\partial x}\left(r^2\frac{\partial\varphi}{\partial x}\right). \tag{21}$$

Substitution of $\partial\rho/\partial t$ into Eq. (20) yields

$$\frac{\partial^2\varphi}{\partial t^2}+\frac{1}{2}\frac{\partial}{\partial t}\left(\frac{\partial\varphi}{\partial x}\right)^2=\frac{\gamma p_0}{\rho_0^{\gamma}}\,\rho^{(\gamma-2)}\left[\frac{\partial\rho}{\partial x}\frac{\partial\varphi}{\partial x}+\frac{\rho}{r^2}\frac{\partial}{\partial x}\left(r^2\frac{\partial\varphi}{\partial x}\right)\right]-\frac{da}{dt}\,x+\frac{\delta}{r^2}\frac{\partial^2}{\partial t\,\partial x}\left(r^2\frac{\partial\varphi}{\partial x}\right). \tag{22}$$

The derivative $\partial\rho/\partial x$ is eliminated from Eq. (22) by differentiation of Eq. (14) with respect to x

$$\frac{\partial^2\varphi}{\partial x\partial t}+\frac{1}{2}\frac{\partial}{\partial x}\left(\frac{\partial\varphi}{\partial x}\right)^2=-\frac{\gamma p_0}{\rho_0^{\gamma}}\,\rho^{(\gamma-2)}\frac{\partial\rho}{\partial x}-a(t). \tag{23}$$

The dissipative term is dropped because $\partial\rho/\partial x$ appears only in the nonlinear term in Eq. (22). According to Eq. (23) $\partial\rho/\partial x$ is

$$\frac{\partial\rho}{\partial x}=-\left(\frac{\gamma p_0}{\rho_0^{\gamma}}\,\rho^{(\gamma-2)}\right)^{-1}\left[\frac{\partial^2\varphi}{\partial x\,\partial t}+\frac{1}{2}\frac{\partial}{\partial x}\left(\frac{\partial\varphi}{\partial x}\right)^2+a(t)\right]. \tag{24}$$

Substituting Eq. (24) into Eq. (22) we obtain

$$\frac{\partial^2\varphi}{\partial t^2}+\frac{1}{2}\frac{\partial}{\partial t}\left(\frac{\partial\varphi}{\partial x}\right)^2=-\left[\frac{\partial^2\varphi}{\partial x\,\partial t}+\frac{1}{2}\frac{\partial}{\partial x}\left(\frac{\partial\varphi}{\partial x}\right)^2+a(t)\right]\frac{\partial\varphi}{\partial x}+\frac{\gamma p_0}{\rho_0^{\gamma}r^2}\,\rho^{(\gamma-1)}\frac{\partial}{\partial x}\left(r^2\frac{\partial\varphi}{\partial x}\right)-\frac{da}{dt}\,x+\frac{\delta}{r^2}\frac{\partial^2}{\partial t\,\partial x}\left(r^2\frac{\partial\varphi}{\partial x}\right). \tag{25}$$

Using Eq. (16) we present Eq. (25) in the form

$$\frac{\partial^2\varphi}{\partial t^2}+\frac{1}{2}\frac{\partial}{\partial t}\left(\frac{\partial\varphi}{\partial x}\right)^2=-\left[\frac{\partial^2\varphi}{\partial x\,\partial t}+\frac{1}{2}\frac{\partial}{\partial x}\left(\frac{\partial\varphi}{\partial x}\right)^2+a(t)\right]\frac{\partial\varphi}{\partial x}+\frac{c^2}{r^2}\frac{\partial}{\partial x}\left(r^2\frac{\partial\varphi}{\partial x}\right)-\frac{da}{dt}\,x+\frac{\delta}{r^2}\frac{\partial^2}{\partial t\,\partial x}\left(r^2\frac{\partial\varphi}{\partial x}\right). \tag{26}$$

Propagation speed c^2 is eliminated from Eq. (26) by Eq. (19) to yield

$$c^2=c_0^2-(\gamma-1)\left[\frac{\partial\varphi}{\partial t}+\frac{1}{2}\left(\frac{\partial\varphi}{\partial x}\right)^2+a(t)x\right]. \tag{27}$$

Again, the dissipative term is dropped. After substituting Eq. (27) into Eq. (26) we obtain

$$\frac{c_0^2}{r^2}\frac{\partial}{\partial x}\left(r^2\frac{\partial\varphi}{\partial x}\right)-\frac{\partial^2\varphi}{\partial t^2}+\frac{\delta}{r^2}\frac{\partial^2}{\partial t\,\partial x}\left(r^2\frac{\partial\varphi}{\partial x}\right)=\frac{da}{dt}\,x+a(t)\,\frac{\partial\varphi}{\partial x}+\frac{\gamma-1}{r^2}\,a(t)x\,\frac{\partial}{\partial x}\left(r^2\frac{\partial\varphi}{\partial x}\right)+2\frac{\partial^2\varphi}{\partial x\,\partial t}\frac{\partial\varphi}{\partial x}+\frac{\gamma-1}{r^2}\frac{\partial\varphi}{\partial t}\frac{\partial}{\partial x}\left(r^2\frac{\partial\varphi}{\partial x}\right)+\frac{1}{3}\frac{\partial}{\partial x}\left(\frac{\partial\varphi}{\partial x}\right)^3+\frac{\gamma-1}{2r^2}\left(\frac{\partial\varphi}{\partial x}\right)^2\frac{\partial}{\partial x}\left(r^2\frac{\partial\varphi}{\partial x}\right). \tag{28}$$

Equation (28) describes the nonlinear standing waves in the resonator of axisymmetric, but otherwise arbitrary shape. The resonator shape is given by the function $r=r(x)$. Oscillation of the entire resonator is characterized by the acceleration $a(t)$. The approximations used in the derivation are that the acoustic attenuation is small so that the nonlinear terms with dissipation are dropped, and that the coefficients of viscosity are constant. During the derivation, energy dissipation in the volume is taken into account. Although the energy losses in the boundary layer are not considered here, they are taken into account by an effective absorption coefficient whose value is greater than the volume dissipation. It is interesting to note that for a perfect gas the dynamic equations are reduced to the single equation for the velocity potential. The equation includes only quadratic and cubic nonlinear terms in spite of the fact that one of the original equations, Eq. (12), has the nonlinearity as ρ^{γ}.

For $a(t)=0$ and for an ideal gas without losses, $\delta=0$, Eq. (28) takes the form

$$\frac{c_0^2}{r^2}\frac{\partial}{\partial x}\left(r^2\frac{\partial\varphi}{\partial x}\right)-\frac{\partial^2\varphi}{\partial t^2}=2\frac{\partial^2\varphi}{\partial x\,\partial t}\frac{\partial\varphi}{\partial x}+\frac{\gamma-1}{r^2}\frac{\partial\varphi}{\partial t}\frac{\partial}{\partial x}\left(r^2\frac{\partial\varphi}{\partial x}\right)+\frac{1}{3}\frac{\partial}{\partial x}\left(\frac{\partial\varphi}{\partial x}\right)^3+\frac{\gamma-1}{2r^2}\left(\frac{\partial\varphi}{\partial x}\right)^2\frac{\partial}{\partial x}\left(r^2\frac{\partial\varphi}{\partial x}\right). \tag{29}$$

Equation (29) is the exact equation for the axisymmetric resonator of an arbitrary shape filled with a lossless perfect gas.

For the resonator of constant radius Eq. (29) is reduced to

$$c_0^2\frac{\partial^2\varphi}{\partial x^2}-\frac{\partial^2\varphi}{\partial t^2}=2\frac{\partial^2\varphi}{\partial x\,\partial t}\frac{\partial\varphi}{\partial x}+(\gamma-1)\frac{\partial\varphi}{\partial t}\frac{\partial^2\varphi}{\partial x^2}+\frac{1}{3}\frac{\partial}{\partial x}\left(\frac{\partial\varphi}{\partial x}\right)^3+\frac{\gamma-1}{2}\left(\frac{\partial\varphi}{\partial x}\right)^2\frac{\partial^2\varphi}{\partial x^2}. \tag{30}$$

Equation (30) coincides with Eq. (26) in Chapter 3 of *Model Equations* by Hamilton and Morfey.[13]

II. PREPARATION FOR NUMERICAL CALCULATIONS

Since the problem is solved numerically, some transformations are required to introduce dimensionless variables, to reduce the order of Eq. (28), and to replace the time domain equations with spectral ones.

A. Dimensionless variables

For numerical purposes it is better to write Eq. (28) in dimensionless form. The dimensionless variables are

$$X=\frac{x}{l},\quad T=\omega t,\quad R=\frac{r}{l},\quad A=\frac{a}{l\omega_0^2},\quad \Phi=\frac{\varphi}{l^2\omega_0}, \tag{31}$$

where l is the length of the resonator, ω is the angular frequency of the periodic force that shakes the resonator, and ω_0 is the frequency of the lowest mode of a cylindrical resonator of length l. The frequency ω_0 is equal to

$$\omega_0=\frac{\pi c_0}{l}. \tag{32}$$

In the dimensionless variables Eq. (28) takes the form

$$\frac{1}{\pi^2R^2}\frac{\partial}{\partial X}\left(R^2\frac{\partial\Phi}{\partial X}\right)-\Omega^2\frac{\partial^2\Phi}{\partial T^2}+\frac{G\Omega}{\pi^3R^2}\frac{\partial^2}{\partial T\,\partial X}\left(R^2\frac{\partial\Phi}{\partial X}\right)=\Omega\frac{dA}{dT}X+A(T)\frac{\partial\Phi}{\partial X}+\frac{\gamma-1}{R^2}A(T)X\frac{\partial}{\partial X}\left(R^2\frac{\partial\Phi}{\partial X}\right)+2\Omega\frac{\partial^2\Phi}{\partial X\,\partial T}\frac{\partial\Phi}{\partial X}+\frac{(\gamma-1)\Omega}{R^2}\frac{\partial\Phi}{\partial T}\frac{\partial}{\partial X}\left(R^2\frac{\partial\Phi}{\partial X}\right)+\frac{1}{3}\frac{\partial}{\partial X}\left(\frac{\partial\Phi}{\partial X}\right)^3+\frac{\gamma-1}{2R^2}\left(\frac{\partial\Phi}{\partial X}\right)^2\frac{\partial}{\partial X}\left(R^2\frac{\partial\Phi}{\partial X}\right). \tag{33}$$

Here the new notations, Ω and G, are introduced

$$\Omega=\frac{\omega}{\omega_0},\quad G=\frac{\pi\delta\omega_0}{c_0^2}. \tag{34}$$

In numerical calculations the different dimensionless attenuation coefficient G_1 has been taken

$$G_1=G\Omega_0. \tag{35}$$

Here, Ω_0 is a frequency in the middle of the narrow frequency interval we work with. As a rule, it is a resonance frequency. The value G_1 makes physical sense, it is equal to

$$G_1=\frac{\lambda}{L}, \tag{36}$$

where λ is the wavelength that corresponds to the resonance frequency, and L is the attenuation length which is reciprocal to the attenuation coefficient α for the same frequency

$$L=\frac{1}{\alpha},\quad \alpha=\frac{\delta\omega^2}{2c_0^3}. \tag{37}$$

B. New variables

To reduce Eq. (33) to a set of differential equations that would contain only the first derivatives with respect to X, a new variable is introduced

$$V=R^2\frac{\partial\Phi}{\partial X}. \tag{38}$$

Multiplying all terms of Eq. (33) by R^2 and performing some transformations we obtain the set of two equations

$$\frac{1}{\pi^2}\frac{\partial V}{\partial X}-\Omega^2R^2\frac{\partial^2\Phi}{\partial T^2}+\frac{G\Omega}{\pi^3}\frac{\partial^2V}{\partial T\,\partial X}=\Omega\frac{dA}{dT}XR^2+AV+(\gamma-1)AX\frac{\partial V}{\partial X}+\frac{\Omega}{R^2}\frac{\partial V^2}{\partial T}+(\gamma-1)\Omega\frac{\partial\Phi}{\partial T}\frac{\partial V}{\partial X}+\frac{\gamma+1}{2R^4}V^2\frac{\partial V}{\partial X}-\frac{2}{R^5}\frac{dR}{dX}V^3, \tag{39}$$

and

$$\frac{\partial \Phi}{\partial X} = \frac{V}{R^2}. \tag{40}$$

Equations (39) and (40) should be transformed to frequency domain.

C. Frequency domain equations

The acceleration is assumed to be periodic and can be presented in the form

$$A = \sum_{k=-N}^{N} A_k e^{ikT}. \tag{41}$$

Here A_k are the complex amplitudes of harmonic components of the acceleration, and $A_{-k} = A_k^*$, where A_k^* are complex conjugates to A_k.

The periodic solutions of Eqs. (39) and (40) are

$$V = \sum_{k=-N}^{N} V_k e^{ikT}, \tag{42}$$

$$\Phi = \sum_{k=-N}^{N} \Phi_k e^{ikT}. \tag{43}$$

Here, V_k are the complex amplitudes of the harmonic components of the function V, $V_{-k} = V_k^*$, where the functions V_k^* are complex conjugates, and $V_0 = V_{\mathrm{dc}}$ is the dc component of the function V. The functions Φ_k are the complex amplitudes of the harmonic components of the velocity potential wave. The functions Φ_{-k} are equal to Φ_k^* where the functions Φ_k^* are complex conjugates. The function $\Phi_0 = \Phi_{\mathrm{dc}}$ is the dc component of the velocity potential. N is the number of harmonics included. Both functions V_{dc} and Φ_{dc} are real. All of the complex amplitudes V_k and Φ_k as well as real functions V_{dc} and Φ_{dc} depend only on X. So Eqs. (39) and (40) are replaced by ordinary differential equations for the complex amplitudes of the harmonic components. The equations for the k component are

$$\begin{aligned}
&\frac{1}{\pi^2}\frac{dV_k}{dX} + k^2\Omega^2 R^2 \Phi_k + \frac{ikG\Omega}{\pi^3}\frac{dV_k}{dX} \\
&\quad = ik\Omega R^2 X A_k + \frac{ik\Omega}{R^2}[V^2]_k \\
&\qquad + \sum_{l=-N+k}^{N} \left\{ A_{k-l} V_l + (\gamma-1) X A_{k-l} \frac{dV_l}{dX} \right. \\
&\qquad \left. + i(k-l)(\gamma-1)\Omega \Phi_{k-l} \frac{dV_l}{dX} \right\} \\
&\qquad + \sum_{l=-N}^{N} \left\{ \frac{\gamma+1}{2R^4}[V^2]_{k-l} \frac{dV_l}{dX} - \frac{2}{R^5}\frac{dR}{dX}[V^2]_{k-l} V_l \right\},
\end{aligned} \tag{44}$$

$$\frac{d\Phi_k}{dX} = \frac{V_k}{R^2}. \tag{45}$$

The index k varies from 0 to N, and the term $[V^2]_k$ is

$$[V^2]_k = \sum_{l=-N+k}^{N} V_{k-l} V_l, \tag{46}$$

where the index k takes values from 0 to $2N$. Equation (44) in matrix form is

$$D_{kl}\frac{dV_l}{dX} = F_k. \tag{47}$$

As follows from Eq. (44), the matrix D_{kl} and the function F_k are equal

$$D_{kl} = \left(\frac{1}{\pi^2} + \frac{ikG\Omega}{\pi^3} \right) \delta_{kl} + D'_{k-l}, \tag{48}$$

$$\begin{aligned}
F_k = &-k^2\Omega^2 R^2 \Phi_k + ik\Omega R^2 X A_k + \frac{ik\Omega}{R^2}[V^2]_k \\
&+ \sum_{l=-N+k}^{N} \{A_{k-l} V_l\} - \frac{2}{R^5}\frac{dR}{dX}\sum_{l=-N}^{N} \{[V^2]_{k-l} V_l\},
\end{aligned} \tag{49}$$

where δ_{kl} is the Kronecker delta function, and D'_m is

$$D'_m = -(\gamma-1) X A_m - im(\gamma-1)\Omega \Phi_m - \frac{\gamma+1}{2R^4}[V^2]_m. \tag{50}$$

Note that

$$D'_{-m} = (D'_m)^*, \quad F_{-k} = F_k^*. \tag{51}$$

Equations (47) and (45) are integrated numerically.

D. Algorithm for numerical calculation

First the derivatives dV/dX are expressed from Eq. (47) as

$$\frac{dV_l}{dX} = S_l(V_k, \Phi_k, X). \tag{52}$$

Here, S_l are functions that are obtained from the solution of Eqs. (47). The functions S_l can be calculated analytically because Eqs. (47) are the linear equations with respect to dV/dX, but we calculate them numerically.

Putting together Eqs. (52) and (45) we have a set of $(4N+1)$ coupled first order ordinary differential equations in real variables. These equations can be solved with a Runge–Kutta method. The boundary conditions are given at $X=0$ and $X=1$ (i.e., on the ends of the resonator). There are $(4N+1)$ equations for the boundary conditions. They are

$$V_k = 0, \quad V_{\mathrm{dc}} = 0, \quad \text{at} \quad X = 0, \tag{53}$$

$$V_k = 0, \quad \text{at} \quad X = 1. \tag{54}$$

The condition $V_{\mathrm{dc}} = 0$ at $X=1$ is satisfied automatically if Eqs. (53) are true, and the mass conservation law is satisfied.

In this particular case the fifth-order Runge–Kutta formulas with adaptive stepsize control[14] are applied to the two-point boundary value problem with $(2N+1)$ known functions at $X=0$ and $2N$ given functions at $X=1$.

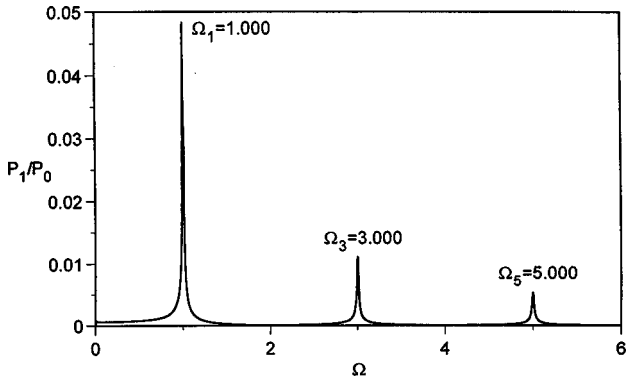

FIG. 1. Response of the cylindrical resonator to the periodic external force that drives the entire resonator with the acceleration amplitude $\tilde{A}=1\times10^{-4}$. Here $N=3$, $G_1=1\times10^{-2}$, and $\gamma=1.2$.

When the functions V_k and Φ_k are obtained, any acoustical variable of interest may be calculated. In particular, the pressure and density in the resonator are evaluated with the following equations:

$$\frac{P}{P_0}=\left[1-(\gamma-1)\pi^2\left(\Omega\,\frac{\partial\Phi}{\partial T}+\frac{1}{2R^4}\,V^2+AX-\frac{G}{\pi^3R^2}\,\frac{\partial V}{\partial X}\right)\right]^{\gamma/(\gamma-1)}, \tag{55}$$

$$\frac{\rho}{\rho_0}=\left[1-(\gamma-1)\pi^2\left(\Omega\,\frac{\partial\Phi}{\partial T}+\frac{1}{2R^4}\,V^2+AX-\frac{G}{\pi^3R^2}\,\frac{\partial V}{\partial X}\right)\right]^{1/(\gamma-1)}. \tag{56}$$

A Fourier transform of the function $P(T,X)$ given by Eq. (55) yields the amplitudes of the harmonic components of the pressure for a certain fixed value X.

III. NUMERICAL RESULTS

Numerical results are presented for three resonators: a cylinder, a cone, and a bulb. The acceleration is assumed to be harmonic. So there is only one harmonic component in the acceleration that is given by the following equation:

$$A(T)=\tilde{A}\cos T. \tag{57}$$

The coefficients A_k in Eq. (41) are

$$A_1=\tilde{A}/2,\quad A_k=0\ \text{ for }\ k>1. \tag{58}$$

In calculations, different values of γ have been taken: $\gamma=1.4$, $\gamma=1.2$, $\gamma=1.15$, and $\gamma=1.1$.

A. Cylindrical resonator

The frequency response of the cylindrical resonator to the periodic acceleration is shown in Fig. 1. The acceleration of the resonator is relatively small, $\tilde{A}=1\times10^{-4}$, so that we operate in the linear region. The cylindrical resonator is a consonant resonator: all the resonance frequencies are integer multiples of the fundamental frequency; i.e., the modes of a cylindrical resonator are equidistant. Note that only odd modes are excited while the even modes are not. For a cylinder, the entire resonator drive can only deliver power when the dynamic pressures at the two opposite ends are out of phase.

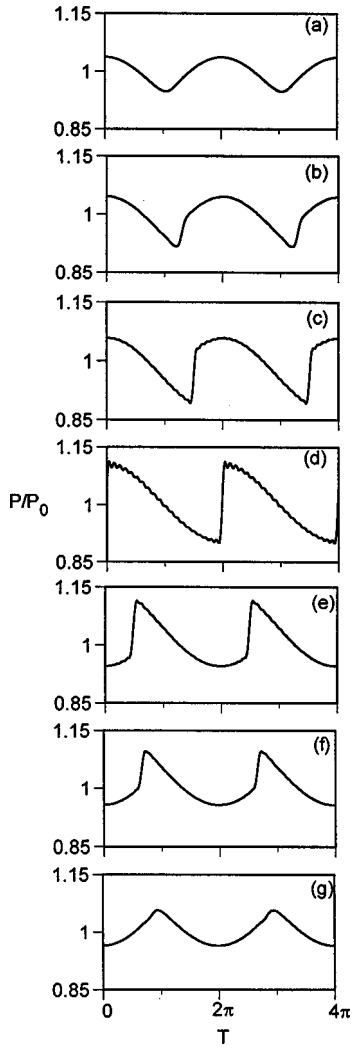

FIG. 2. The wave shapes of the pressure wave near the resonance frequency in the cylindrical resonator: the top three shapes are before resonance: $\Omega=0.970$ (a), $\Omega=0.975$ (b), and $\Omega=0.980$ (c), the fourth waveform corresponds to the resonance frequency $\Omega=1.0$ (d), and the lower three shapes are after resonance: $\Omega=1.020$ (e), $\Omega=1.025$ (f), and $\Omega=1.030$ (g). Here $\tilde{A}=5\times10^{-4}$, $N=20$, $G_1=1\cdot10^{-2}$, $\gamma=1.2$.

Changes of the shape of the pressure wave in a cylindrical resonator are very strong near the resonance frequency ($\Omega=1$). Several waveforms calculated at $X=0$ for $\tilde{A}=5\times10^{-4}$ are shown in Fig. 2. The upper three plots (a), (b), and (c) display pressure wave shapes below resonance. The fourth plot (d) corresponds to the resonance frequency $\Omega=1$. The lower three plots (e), (f), and (g) demonstrate the waveform above resonance. The dimensionless attenuation coefficient is $G_1=1\times10^{-2}$. This value of the attenuation coefficient is chosen in order to obtain a Q-factor that is close to the value of the Q-factor of the cylindrical resonator measured by experiment.[1] The Q-factor is expressed through the attenuation coefficient as

$$Q=\frac{\pi}{G_1}. \tag{59}$$

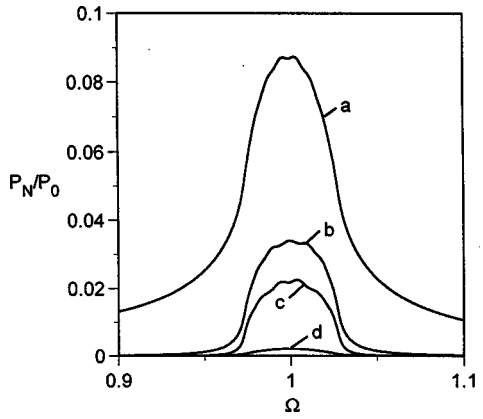

FIG. 3. Frequency response of the pressure amplitudes of the fundamental (curve a), second (curve b), and third (curve c) harmonic components, as well as the dc component (curve d) in the cylindrical resonator. Here $\tilde{A}=5\times10^{-4}$, $N=10$, $G_1=1\times10^{-2}$, $\gamma=1.2$.

The evolution of the waveform shapes agree well with the prediction by Chester[5] and the measurements by Cruikshank[6] and MacroSonix.[1] At low frequencies the cusps appear at the bottom part of the waveform, while for high frequencies cusps appear at the top. In the calculation 20 harmonics are taken into account.

Figure 3 shows the dependence of the amplitudes of the first three harmonics [curves (a), (b), and (c)] and dc component [curve (d)] on the external force frequency. Here the acceleration is $\tilde{A}=5\times10^{-4}$, and the amplitudes are calculated at $X=0$. The dc component is very small.

When the acceleration is increased, the amplitudes of all harmonic components are getting larger, but the resonance curves are getting broader. The intense harmonic generation at the high amplitude introduces additional attenuation that results in a decreasing ''*Q*-factor.'' This can be seen in Fig. 4, where the resonance curve of the fundamental pressure wave is shown for different amplitudes of the acceleration: $\tilde{A}=5\times10^{-4}$ [curve (a)], $\tilde{A}=2.5\times10^{-4}$ [curve (b)], and $\tilde{A}=1\times10^{-4}$ [curve (c)]. From the calculations it is also obvious that there is no significant resonance frequency shift (softening or hardening behavior) noticeable with increasing

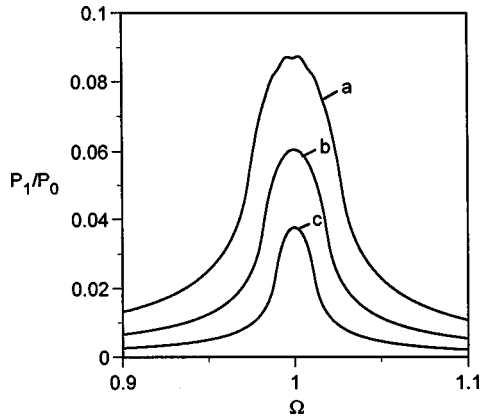

FIG. 4. Frequency response of the fundamental pressure wave in the cylindrical resonator for different acceleration amplitudes: $\tilde{A}=5\times10^{-4}$ (curve a), $\tilde{A}=2.5\times10^{-4}$ (curve b), and $\tilde{A}=1\times10^{-4}$ (curve c). Here $N=10$, $G_1=1\times10^{-2}$, $\gamma=1.2$.

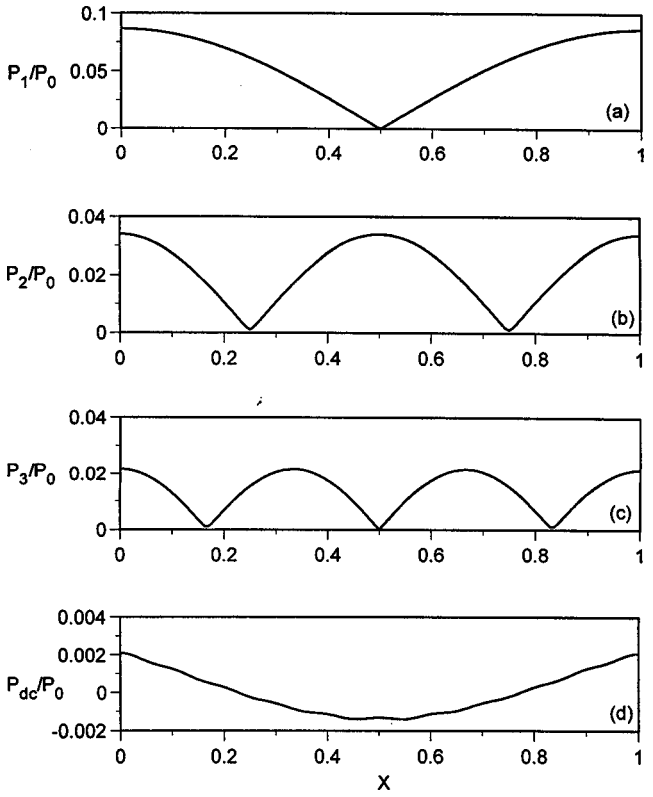

FIG. 5. Amplitude distributions of the fundamental pressure wave (a), the second (b), and third harmonics (c), as well as the dc component (d) along the cylindrical resonator axis. Here $\tilde{A}=5\times10^{-4}$, $N=10$, $G_1=1\times10^{-2}$, $\gamma=1.2$.

amplitude: the resonance curve is not skewed; it remains symmetric, and the maximum response is always obtained at $\Omega=1$. A similar behavior is obtained for the second and third harmonic, where no hardening or softening is observed. Cruikshank[6] presents evidence of a fairly small hard spring behavior for oscillations in a tube excited by a piston. Coppens and Sanders show that the response of the second and third harmonic increases slightly (on the order of 0.2%) with amplitude. In both cases, it is possible that this is caused by the difference in excitation mechanism, i.e., single piston motion in Cruikshank's and Coppens and Sanders' experiment versus entire resonator driving in this model. However, the small increase in resonance frequency observed by Cruikshank and Coppens and Sanders could also be explained by an increase in ambient temperature of the gas inside the tube caused by a higher energy dissipation at higher drive amplitudes. The increase in ambient temperature inside the tube raises the speed of sound at the rate of 0.17% per deg Celsius increase for a 20 deg Celsius tube. In the experiments performed by MacroSonix,[1] no significant hardening or softening is observed, in agreement with the results reported here.

Pressure distributions along the cylindrical resonator axis for $\tilde{A}=5\times10^{-4}$ and $\Omega=1$ are plotted in Fig. 5 for the fundamental component (a), the second harmonic (b), and third harmonic amplitudes (c), as well as for the dc component (d).

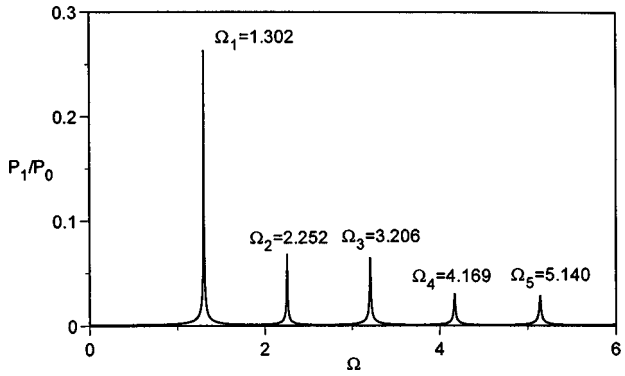

FIG. 6. Response of the conical resonator to the periodical external force that drives the entire resonator with the acceleration amplitude $\tilde{A}=1\times10^{-4}$. Here $N=3$, $G_1=1\times10^{-2}$, $\gamma=1.2$.

B. Conical resonator

The geometry of the conical resonator is

$$r(x)=0.0056+0.2680\cdot x, \quad \text{for} \quad 0\leqslant x\leqslant 0.17 \text{ m}, \quad (60)$$

where r is the radius in meters and x is the coordinate along the resonator axis.

The frequency response of the conical resonator to the periodic acceleration is shown in Fig. 6. Again, the acceleration of the resonator is small, $\tilde{A}=1\times10^{-4}$, so that this closely approximates the linear case. The conical resonator is an example of a dissonant resonator. As seen in Fig. 6, the higher resonance frequencies are not integer multiples of the fundamental frequency.

For high amplitudes of oscillation, for example, when $\tilde{A}=5\times10^{-4}$, hysteresis takes place in the conical resonator. Figure 7 displays the dependence of the fundamental pressure wave amplitude [curves (a)] and the second harmonic [curves (b)] on the frequency: the upper branches are obtained when frequency increases (sweep up), and lower curves correspond to decreasing frequency (sweep down). There are some frequencies where P_1 and P_2 are double valued. The conical resonator behaves as a hard spring, the resonance frequency increases with increasing amplitude. The hardening behavior is very pronounced, and it is very different from that of the cylindrical resonator.

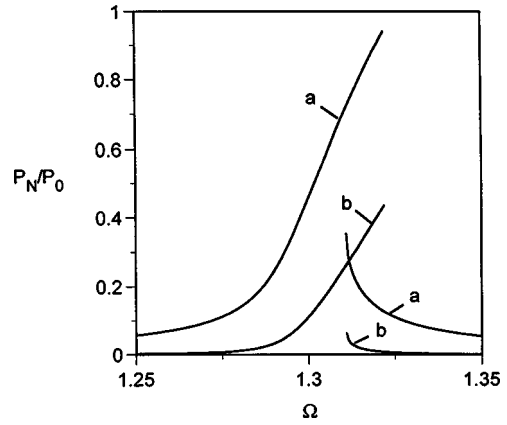

FIG. 7. Frequency responses of the pressure amplitudes of the fundamental (curves a) and second (curves b) harmonic components in the conical resonator. Here $\tilde{A}=5\times10^{-4}$, $N=10$, $G_1=1\times10^{-2}$, $\gamma=1.2$.

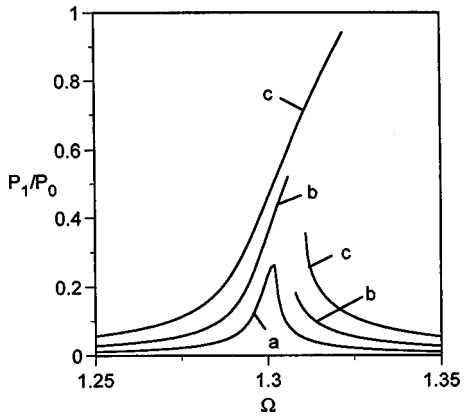

FIG. 8. Frequency responses of the fundamental pressure wave in the conical resonator for different acceleration amplitudes: $\tilde{A}=1\times10^{-4}$ (curve a), $\tilde{A}=2.5\times10^{-4}$ (curves b), and $\tilde{A}=5\times10^{-4}$ (curves c). Here $N=10$, $G_1=1\times10^{-2}$, $\gamma=1.2$.

In Fig. 8 the dependence of the fundamental wave amplitude on frequency is shown for three different amplitudes of the acceleration of the conical resonator. There is no hysteresis for $\tilde{A}=1\times10^{-4}$ [curve (a)]. When $\tilde{A}=2.5\times10^{-4}$ the resonance curve is skewed to the right but the upper and the lower branches are not overlapped [curves (b)]. For $\tilde{A}=5\times10^{-4}$, a multi-valued function is obtained [curves (c)].

Figure 9 shows the pressure waveform at $X=0$ for $\tilde{A}=5\times10^{-4}$ and for the frequency $\Omega=1.325$, at which the maximum pressure response is obtained for the sweep up calculation. The waveform does not resemble a sawtooth shape at all, and has a smooth signal that does not contain any shocks. The waveform has a broad bottom part and a peaked top. The peak pressure is about 3.2 and the minimum pressure is about 0.5, so that a pressure ratio of 6.4 is achieved. This is more than five times the pressure ratio obtained in the cylindrical resonator (see Fig. 2), where the peak pressure is 1.1, the minimum pressure is 0.9, and the pressure ratio is 1.22.

The pressure distributions along the conical resonator are shown in Fig. 10 for the amplitudes of the first three harmonic components [(a), (b), (c)] and the dc pressure (d). The parameters are $\tilde{A}=5\times10^{-4}$, $\Omega=1.325$.

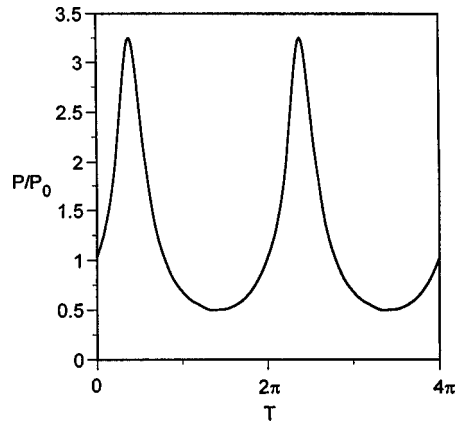

FIG. 9. The wave shape of the pressure wave at frequency $\Omega=1.325$ in the conical resonator. Here $\tilde{A}=5\times10^{-4}$, $N=10$, $G_1=1\times10^{-2}$, $\gamma=1.2$.

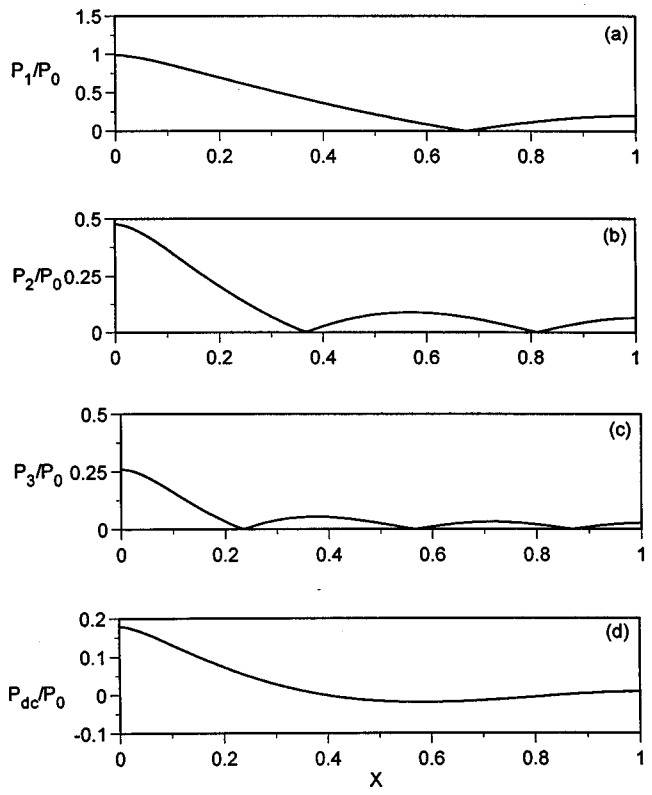

FIG. 10. Amplitude distributions of the fundamental pressure wave (a), the second (b), and third harmonic (c), as well as the dc component (d) along the conical resonator axis. Here $\tilde{A}=5\times10^{-4}$, $\Omega=1.325$, $N=10$, $G_1=1\times10^{-2}$, $\gamma=1.2$.

For the calculation of the conical resonator ten harmonics are taken into account, and the attenuation coefficient is $G_1=1\times10^{-2}$ which gives the ''Q-factor'' that is close to the value measured by experiment.

From Fig. 10 it is seen that the pressure amplitude of the fundamental component at the throat, the narrow end of the resonator at $X=0$, is about five times higher than the pressure at the mouth, the wide end at $X=1$. For the conical resonator the dc pressure amplitude at the throat is much bigger than for the cylinder, a dc pressure value of 0.18 versus 0.002.

From Fig. 10, one sees that at the narrow end the amplitude of the fundamental wave is $P_1/P_0=0.99$, the second harmonic is $P_2/P_0=0.48$, and the third is $P_3/P_0=0.26$. It is interesting to note that high amplitudes of the fundamental wave and harmonics can be achieved without the presence of a shock in the waveform.

C. Bulb resonator

In this section, the strong influence of the resonator shape on the acoustical field inside the resonator is demonstrated. As shown in Fig. 11, two very similar resonators are considered: both of them are bulbs, one has a flare at the narrow end, as seen in Fig. 11(a), and the second one in Fig. 11(b) has no flare. Frequency responses of both resonators are shown in Fig. 12, where (a) corresponds to the bulb with a flare, and (b) to the bulb without a flare. The resonator with a flare has a slightly lower fundamental resonance frequency, but a significantly lower second and third resonance frequency. The hysteresis effects are different for the resonators. Both of these resonators display a softening behavior, i.e., the fundamental resonance frequency decreases with increasing amplitude, but for the bulb with the flare a very pronounced hysteresis is apparent, while for the resonator without a flare no hysteresis is present. The softening behavior for the resonator with a flare is shown in Fig. 13 for three values of the acceleration: there is no hysteresis for $\tilde{A}$

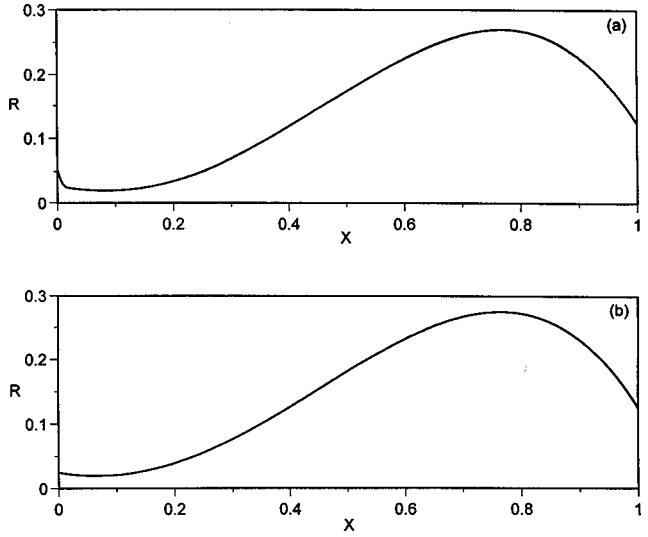

FIG. 11. Two bulb resonators: the bulb with a flare (a) and the bulb without a flare (b).

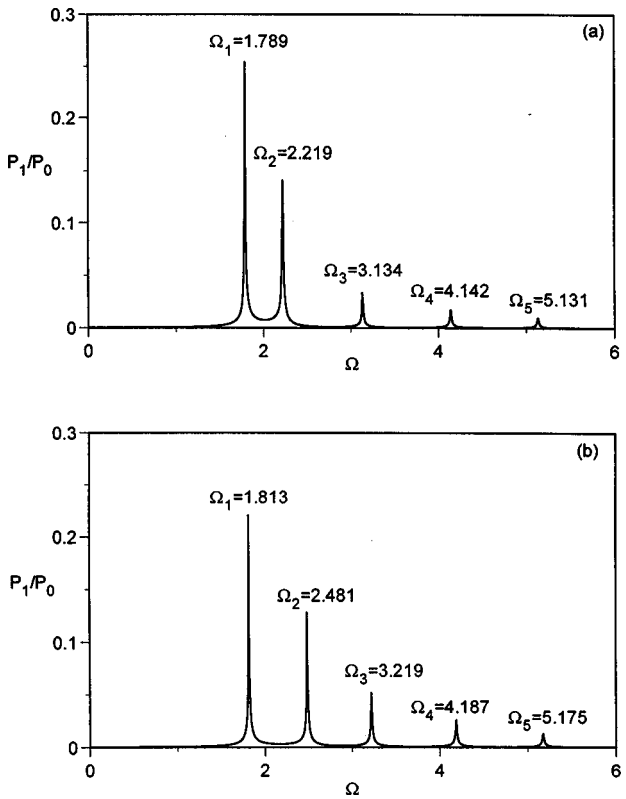

FIG. 12. Responses of two bulb resonators with the flare (a) and without flare (b) to the periodical external force that drives each of them with the acceleration amplitude $\tilde{A}=0.5\times10^{-4}$. Here $N=3$, $G_1=0.5\times10^{-2}$, $\gamma=1.2$.

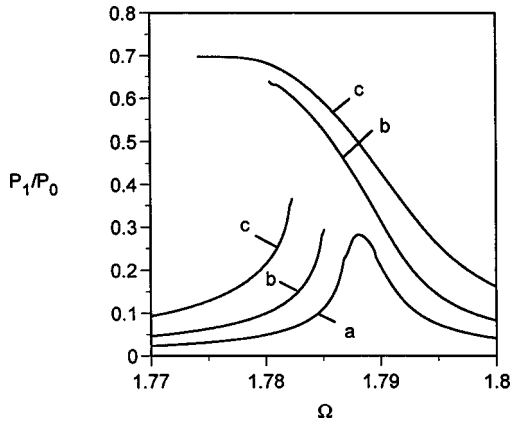

FIG. 13. Frequency responses of the fundamental pressure wave in the bulb with a flare for different acceleration amplitudes: $\tilde{A}=0.25\times10^{-4}$ (curve a), $\tilde{A}=0.5\times10^{-4}$ (curves b), and $\tilde{A}=1\times10^{-4}$ (curves c). Here $N=10$, $G_1=0.5\times10^{-2}$, $\gamma=1.2$.

$=0.25\times10^{-4}$ [curve (a)], but the swept up and swept down branches are overlapped for $\tilde{A}=0.5\times10^{-4}$ [curves (b)] and for $\tilde{A}=1\times10^{-4}$ [curves (c)].

It is necessary to emphasize that any axisymmetric geometry can be considered in this model. Besides a cylinder, a cone, and two bulbs we have modeled a horn, a horn cone, and another bulb. Dissonance characterizes all resonators we considered except the cylinder, and results in a phase mismatching between the harmonic components that prevents shock formation.

D. Comparison with experiment

The numerical results obtained with the model are in good agreement with measurements done at MacroSonix[1] and with results known from the literature.[6,7] A detailed quantitative comparison of experimental results with theoretical predictions is beyond the scope of this paper. Qualitatively, the model describes all phenomena observed in the experiments: resonance frequency shift, hysteresis, and waveform distortion.

As measurements and calculations show, the resonance frequency shift depends not only on the amplitude of oscillations but very strongly on the resonator shape. The resonator shape determines the sign of the frequency shift which results in a hardening (increase of the resonance frequency) or softening (decrease of the resonance frequency) behavior. Measurements conducted at MacroSonix[1] showed the same hardening behavior for the conical resonator and the softening behavior for the bulb resonator. For the cylinder, the calculations showed no significant hardening or softening and again this is confirmed by measurements.

The waveform distortion calculated with the model is very similar to that measured. As an example, Fig. 14 demonstrates a measured wave shape (solid line) and a calculated wave shape (dashed line) for the conical resonator. The waveform predicted by the model is in very good agreement with the measurement. In Table I the values of the fundamental, second, and third harmonic amplitudes are shown for the predicted and the measured waveforms.

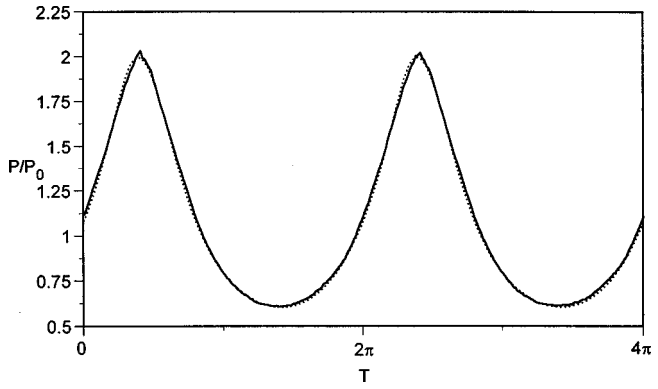

FIG. 14. Comparison of the measured wave shape (the solid line) with the theoretical prediction (the dash line) for the conical resonator. The parameters are $\tilde{A}=2.85\times10^{-4}$, $\Omega=1.31$, $N=10$, $G_1=1\times10^{-2}$, $\gamma=1.1$.

IV. CONCLUSIONS

A one-dimensional mathematical model and a numerical code have been developed for the analysis of nonlinear standing waves in axisymmetric resonators. The model equation is derived from the fundamental gas dynamics equations for an ideal gas. Total nonlinearity of the gas and gasdynamic equations, volume attenuation due to viscosity, entire resonator driving, and dependence of the radius on the coordinate along the resonator are included in the model equation. The model equation is solved numerically in the frequency domain.

Results are presented for a cylindrical, a conical, and a bulb resonator. For the cylinder the results agree well with measurements done at MacroSonix and with predictions and measurements reported in the literature. For moderate to high shaking amplitudes, a shock is formed in the cylinder, and the pressure ratio, ratio of peak pressure to minimum pressure, that can be obtained is very limited. No significant hardening or softening behavior of the cylindrical resonator is observed.

The conical and bulb resonators reveal a different behavior compared to the cylinder. Because of dissonance, harmonic generation is inefficient. Therefore, shock waves are not formed and significant pressure ratios can be achieved. The high pressure ratios and shock-free waveforms create the potential for new applications such as acoustic compressors, pumps, and others. The results of the conical resonator also indicate a very strong hardening behavior while the bulb demonstrates a softening one. At high shaking amplitudes the resonance curves of both cavities are characterized by hysteresis.

Finally, the one-dimensional model presented here can be used as a tool in the design of resonators to create high

TABLE I. Comparison between predicted and measured values of fundamental, second, and third harmonic component amplitudes in a conical resonator.

	P_1/P_0	P_2/P_1	P_3/P_1
Model	0.62	0.31	0.11
Experiment	0.62	0.30	0.09

amplitude standing waves of a given shape and given pressure ratio.

[1] C. Lawrenson, B. Lipkens, T. S. Lucas, D. K. Perkins, and T. W. Van Doren, ''Measurements of macrosonic standing waves in oscillating closed cavities,'' J. Acoust. Soc. Am. **104**, 623–636 (1998).

[2] R. Saenger and G. Hudson, ''Periodic shock waves in resonating gas columns,'' J. Acoust. Soc. Am. **32**, 961–970 (1960).

[3] S. Weiner, ''Standing sound waves of finite amplitude,'' J. Acoust. Soc. Am. **40**, 240–243 (1966).

[4] S. Temkin, ''Propagating and standing sawtooth waves,'' J. Acoust. Soc. Am. **45**, 224–227 (1969).

[5] W. Chester, ''Resonant oscillations in closed tubes,'' J. Fluid Mech. **18**, 44–64 (1964).

[6] D. B. Cruikshank, Jr., ''Experimental investigation of finite-amplitude acoustic oscillations in a closed tube,'' J. Acoust. Soc. Am. **52**, 1024–1036 (1972).

[7] A. B. Coppens and J. V. Sanders, ''Finite-amplitude standing waves in rigid-walled tubes,'' J. Acoust. Soc. Am. **43**, 516–529 (1968).

[8] A. B. Coppens and J. V. Sanders, ''Finite-amplitude standing waves within real cavities,'' J. Acoust. Soc. Am. **58**, 1133–1140 (1975).

[9] D. F. Gaitan and A. A. Atchley, ''Finite amplitude standing waves in harmonic and anharmonic tubes,'' J. Acoust. Soc. Am. **93**, 2489–2495 (1993).

[10] H. Goldstein, *Classical Mechanics* (Addison-Wesley, London, 1981).

[11] A. B. Coppens and A. A. Atchley, ''Nonlinear standing waves in cavities,'' in *Encyclopedia of Acoustics*, edited by M. J. Crocker (Wiley, New York, 1997).

[12] L. D. Landau and E. M. Lifshitz, *Fluid Mechanics* (Pergamon, Oxford, 1987).

[13] M. F. Hamilton and C. L. Morfey, ''Model equations,'' in *Nonlinear Acoustics*, edited by M. F. Hamilton and D. T. Blackstock (Academic, New York, 1997).

[14] W. H. Press, S. A. Teukovsky, W. T. Vetterling, and B. P. Flannery, *Numerical recipes in FORTRAN* (Cambridge U.P., New York, 1992).